Analysis of the Flow in the Boundary Layer of a Marine Propeller Blade Calculated with a RANSE Method

Arnau Jovell Megias
arnau.jovell@tecnico.ulisboa.pt

Instituto Superior Técnico, Universidade de Lisboa, Portugal

February 2021

Abstract

RANSE models have been and are used in Marine and Aeronautical Engineering in CFD investigations for their large potential to predict propeller performances, flow behaviours, and propeller scale effect behaviours. Such is their potential that it is still an on-going area of investigation in many places around the world. In this Thesis, the main objective is to obtain results from RANSE calculations of relevant parameters of the boundary layer in a marine propeller. Two turbulence models are used to predict the performance of the marine propeller P4119, and to compare the results to the experimental data made available by Jessup in 1984. A numerical verification of the results is also made, where the uncertainty and discretization errors are estimated.

The results obtained show a very acceptable value for the uncertainty and errors made, and generally a rather good agreement of the simulated results with the experimental data available. Even though the two models yield similar but different results and after the analysis, the $\gamma - \tilde{Re}_{\theta_t}$ model is considered a more suitable model for this work, since it includes both a laminar and a turbulent region, with the transition region present. The $k - \omega$ SST model is considered not as good in lower Reynolds numbers, but much better for higher Reynolds numbers.
Keywords: Turbulence and transition model, Marine propeller, RANSE, Simulation

1. Introduction

Describing the world in which we live employing the use of mathematics is an action that has been repeatedly done by humanity during –at least– thousands of years. It is not insurmountable to think that we will keep doing this for a very long time after the present day. This work is but a mere iteration of this action, by reproducing the experiments carried out by Stuart D. Jessup et al in 1984 [1], with two different turbulence models widely used in Marine Engineering.

The objectives of this work is to derive from the RANSE calculations the relevant blade boundary layer flow parameters and compare the results with the experimental data obtained by Jessup et al in 1984 [1]. Furthermore, secondary objectives of this work include:

1. Do a literature review on the boundary layer flow on marine propeller blades.
2. Calculate the flow around the propeller P4119, with RANSE code REFRESCO including the effect of transition.
3. Estimate the numerical errors that occur in the simulations.
4. Analyse the propeller blade flow, as well as the parameters of the boundary layer.
5. Gain a deeper understanding of the physics of the flow from the results obtained.

In recent times, turbulence modelling and prediction has been a topic of importance in both Marine and Aeronautical Engineering. Real world turbulence has also very well studied effects on aeronautical and marine equipment. This chapter aims to shed a light on the investigations and studies carried out in these fields. In Marine Engineering, investigations such as [2, 3] study the modification of these turbulence models and how it affects the later results. Other investigations [4, 5] have used this model to accurately predict flow characteristics on different propellers and flow conditions.

The big appeal of turbulence models, though, is studying and predicting scale-effects on propellers, such as the results presented in different

Marine Propeller Symposiums [6, 7] where these models were employed to study the scale-effects and establish relationships between scale-model propellers and full-sized propellers.

In Aeronautical Engineering, other authors have investigated the calibration of turbulence model to better predict turbulence in specific conditions [8, 9], and also perform accurate studies on efficiency optimization on wind turbines. Other investigations have developed hybrid models to predict very complex phenomena that cannot be predicted otherwise [10, 11], like three-dimensional flow separation at a wing junction.

2. Mathematical Models

The turbulence models used in this work are the modified fully turbulent $k-\omega$ SST Model Menter et al [12] and the transition model $\gamma - \tilde{R}e_\theta$ from R. Langtry and F. Menter [13, 14]. The flow equations used are the Reynolds-Averaged Navier-Stokes Equations (RANSE), which are described below.

2.1. RANS Equations

The RANS equations, considering an incompressible, time-invariant flow, can be written in tensor notation as

$$\begin{aligned}&\frac{\partial(\rho V_i)}{\partial X_i} = 0,\\ &\rho\frac{\partial(V_i V_j)}{\partial X_j} + \rho 2\varepsilon_{ijk}\Omega_j V_k + \rho\varepsilon_{ipq}\varepsilon_{qjk}\Omega_p\Omega_j X_k = \\ &= -\frac{\partial P}{\partial X_i} + \frac{\partial}{\partial X_j}\left[(\mu+\mu_t)\left(\frac{\partial V_i}{\partial X_j}+\frac{\partial V_j}{\partial X_i}\right)\right]\end{aligned} \quad (1)$$

Where V_i and X_i are the velocities and coordinates with respect to a non-intertial frame –in this case, rotating with the propeller–, P is the modified static pressure $P = p + 2/3\rho k$, where k is the turbulent kinetic energy and ρ the fluid density. Ω_i is the propeller rotation angular velocity, ε the Levi-Civita symbol and μ and μ_t the fluid's viscosity and turbulent viscosity respectively. To further simplify these equations and condense the Coriolis term and centripetal acceleration term, the earth-fixed velocity is defined as $U_i = V_i + \varepsilon_{ijk}\Omega_j r_k$ and then the RANS equations may be written as

$$\begin{aligned}&\frac{\partial U_i}{\partial X_i} = 0,\\ &\rho\frac{\partial(V_j U_i)}{\partial X_j} + \rho\varepsilon_{ijk}\Omega_j U_k = \\ &= -\frac{\partial P}{\partial X_i} + \frac{\partial}{\partial X_j}\left[(\mu+\mu_t)\left(\frac{\partial U_i}{\partial X_j}+\frac{\partial U_j}{\partial X_i}\right)\right].\end{aligned} \quad (2)$$

2.2. The $k-\omega$ SST model

This model presents two transport equations for the turbulent kinetic energy k and the rate of turbulence dissipation ω:

$$\begin{aligned}&\frac{\partial(\rho U_i k)}{\partial X_i} = \tilde{P}_k - \beta^*\rho k\omega + \frac{\partial}{\partial X_i}\left[(\mu+\sigma_k\mu_t)\frac{\partial k}{\partial X_i}\right],\\ &\frac{\partial(\rho U_i \omega)}{\partial X_i} = \alpha\rho S^2 - \beta\rho\omega^2 + \\ &+ \frac{\partial}{\partial X_i}\left[(\mu+\sigma_\omega\mu_t)\frac{\partial\omega}{\partial X_i}\right] + 2(1-F_1)\rho\sigma_{\omega 2}\frac{1}{\omega}\frac{\partial k}{\partial X_i}\frac{\partial\omega}{\partial X_i},\end{aligned} \quad (3)$$

with a production limiter $\tilde{P}_k = \min(P_k, 10\beta^*\rho k\omega)$ in the k equation given by

$$P_k = \mu_t\frac{\partial U_i}{\partial X_j}\left(\frac{\partial U_i}{\partial X_j}+\frac{\partial U_j}{\partial X_i}\right). \quad (4)$$

On the ω equation there is the blending function F_1 given by

$$F_1 = \tanh\left\{\left\{\min\left[\max\left(\frac{\sqrt{k}}{\beta^*\omega y}, \frac{500\mu}{y^2\omega}\right), \frac{4\rho\sigma_{\omega 2}k}{CD_{k\omega}y^2}\right]\right\}^4\right\} \quad (5)$$

with $CD_{k\omega} = \max\left(2\rho\sigma_{\omega 2}\frac{1}{\omega}\frac{\partial k}{\partial X_i}\frac{\partial\omega}{\partial X_i}, 10^{-10}\right)$ and y being the distance to the nearest wall. This version of the model also includes a modification of the definition of the turbulent viscosity μ_t:

$$\mu_t = \frac{\rho a_1 k}{\max(a_1\omega, SF_2)}, \quad (6)$$

and the second blending function F_2

$$F_2 = \tanh\left\{\left[\max\left(\frac{2\sqrt{k}}{\beta^*,\omega y}, \frac{500\mu}{\rho y^2\omega}\right)\right]^2\right\}. \quad (7)$$

2.3. The $\gamma - \tilde{R}e_\theta$ model

This model presents four equations: two to model turbulence, which are almost identical to the ones of the $k-\omega$ SST model and two more to model the flow transition, one for the intermittency and another one for the transition momentum-thickness Reynolds number:

$$\begin{aligned}&\frac{\partial(\rho U_j\gamma)}{\partial X_j} = P_\gamma - E_\gamma + \frac{\partial}{\partial X_j}\left[\left(\mu+\frac{\mu_t}{\sigma_f}\right)\frac{\partial\gamma}{\partial X_j}\right]\\ &\frac{\partial(\rho U_j\tilde{R}e_{\theta_t})}{\partial x_j} = P_{\theta t} + \frac{\partial}{\partial X_j}\left[\sigma_{\theta t}(\mu+\mu_t)\frac{\partial\tilde{R}e_{\theta_t}}{\partial X_j}\right],\end{aligned} \quad (8)$$

where P_γ is the transition source term based on empirical relations and E_γ is the destruction or relaminarization term. In the same manner, the $\tilde{R}e_\theta$ equation presents a source term $P_{\theta t}$. To fully integrate this model with the SST model, the turbulent kinetic energy equation must be modified with the redefinition of the destruction and source terms:

$$\frac{\partial(\rho k)}{\partial t} + \frac{\partial(\rho U_i k)}{\partial X_i} = \tilde{P}_k - \tilde{D}_k + \frac{\partial}{\partial X_i}\left[(\mu+\sigma_k\mu_t)\frac{\partial k}{\partial X_i}\right] \quad (9)$$

where $\tilde{P}_k$ and $\tilde{D}_k$ are the modified destruction and source terms.

3. Simulations

The simulations performed in this work are based on the P4119 propeller, originally designed by Denny in 1968 [15]. It is a three-bladed propeller with a design advance coefficient of $J = 0.833$ and a diameter of $D_p = 0.305\text{m}$. Since the geometry is the same as the investigation from Baltazar et al [16], the same domain and grids have been used. The grids' number of elements ranges from 1 million to 38 million, to correctly perform a convergence analysis of the results. A summary of the grids is shown in Table 1 below.

Table 1: Characteristics of the grids used.

Grid name	Number of elements	h_i/h_1
1M	$861,381$	3.52
2M	$1,946,304$	2.68
6M	$6,061,608$	1.83
10M	$9,946,965$	1.55
21M	$21,018,771$	1.21
38M	$37,584,261$	1.00

The solver ReFRESCO [17], coupled with the turbulence models is used in all of the simulations performed. The code uses a segregated solution procedure, which solves every equation separately from the others, with a pre-set algorithm, and then couples all equations to check for convergence.

For the purpose of mirroring the data obtained by Jessup, flow parameters have been adjusted according to Table 2 below.

The boundary conditions applied in the simulations are rather standard for a marine propeller. On the inlet the inflow velocity is set according to the value on Table 1 and uniform across the surface. The turbulence intensities (and thus, k) are also set for this boundary condition; $\tilde{Re}_{\theta_t}$ is a function of k, $\gamma = 1$ and the pressure is extrapolated. On the outlet, all streamwise derivatives are set to be zero. On the outer boundary, the pressure is set and all the other variables have the Neumann condition. At the wall, the condition is a no-slip and impermeability condition, and the pressure derivative is zero. $k = 0$, ω is set according to eq. (A12) in [18], and γ and $\tilde{Re}_{\theta_t}$ are set with the Neumann condition.

4. Results & discussion

The results obtained were analysed error-wise, and then compared to the experimental data.

4.1. Iteration error analysis

The iteration errors were analysed to observe iterative convergence. For that purpose, the residuals L_2 and L_∞ were analysed. These residuals are defined as

$$L_2 = \frac{\sqrt{\sum_{i=1}^{N} q_i^2}}{N}$$
$$L_\infty = \max(q_i) \tag{10}$$

where N is the total number of elements and q_i is the residual of a flow variable in element i. These residuals have been plotted for the 38M grid and are shown in Figure 1.

The results show good convergence and the residual value on most parameters is $L < 10^{-6}$, which is acceptable enough for the purpose of this work. The increase in value of some of the residuals corresponds to resets in the simulations.

Besides the residuals, convergence of certain parameters has also been checked, namely the pressure coefficient, the velocity profiles and the thrust and torque coefficients. The first two being a local quantity and the latter ones being a global quantity allows for a wider understanding of the errors generated in the simulations. Selected results are shown in Figure 2. The local quantities were studied at $x/c = 0.2$ and $x/c = 0.8$ chord locations in the suction side.

While convergence is not monotonic for all the parameters involved, it is true that there is indeed convergence and these results are deemed acceptable. The local variables studied showed the most disagreement between models and location of study.

4.2. Discretization error analysis

The other error analysed in the result was the discretization error. This was done with the methodology proposed by Eça and Hoekstra [19, 20] which involves the estimation of the error through the equations

$$\epsilon_\phi = \phi_i - \phi_0 = \alpha h_i^p,$$
$$h_i = \left(\frac{1}{N_{\text{cells}}}\right)^{\frac{1}{3}} \tag{11}$$

where ϕ_i is any integral local flow quantity, ϕ_0 is the estimate of the exact solution of the quantity, α is an unknown constant, h_i is the typical cell size of the considered grid and p is the observed order of grid convergence. With the error estimated, the next step is to estimate the uncertainty U_φ, also included in the method proposed by Eça and Hoekstra. The results of this analysis are shown in Figure 3.

With observed orders of convergence of around $p = 2.00$ for all cases shown, grid convergence is

Table 2: Simulation parameters values.

Parameter	Units	Symbol	Case	
			$Re = 0.73 \times 10^6$	$Re = 1.46 \times 10^6$
Angular speed	rps	n	7	14
Advance velocity	$\mathrm{m/s}$	v_a	1.72081	2.44162
Reference velocity	$\mathrm{m/s}$	v_{ref}	5.00058	9.70246
Dynamic viscosity	$\mathrm{Pa \cdot s}$	μ	9.601×10^{-4}	9.601×10^{-4}
Water density	$\mathrm{kg/m^3}$	ρ	997.83	997.83

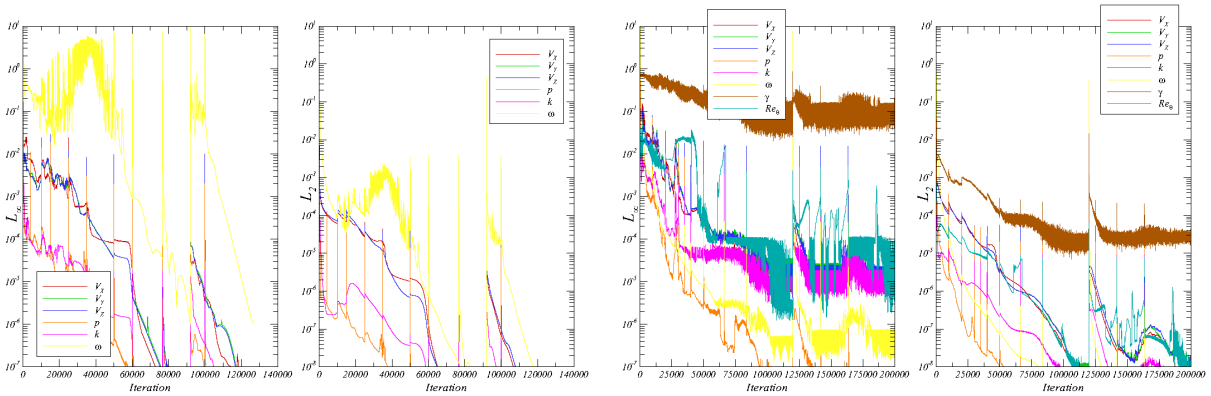

(a) Residuals L_∞ and L_2 for the $k-\omega$ SST2003 model obtained with the 38M grid.

(b) Residuals L_∞ and L_2 for the $\gamma - \tilde{Re}_{\theta t}$ model with $Tu = 1.5\%$, obtained with the 38M grid.

Figure 1: Residuals versus iterations for the two models studied and the 38M grid.

considered more than acceptable, as well as uncertainty values well below 1%. These results paint a very positive picture for the trust put in the results, and what remains to be seen is the comparation with the experimental values.

4.3. Comparison with experimental

On the comparison of the experimental results with the simulated ones, several parameters were studied. These were the pressure coefficient, the velocity profiles, the boundary layer displacement thickness and shape factor, and the flow's streamlines on the propeller blades. It is worth noting that this last parameter was compared in a qualitative way with photos from paint-tests.

The pressure coefficient, shown in Figure 4a, shows little to no variation between models and cases presented, and has a general agreement with the experimental data. The largest difference lies near the trailing edge region of the pressure side, where the models predict a decrease in pressure while the experimental data does not.

The velocity profiles do not show the same level of agreement, though. The differences between the models and even between different cases of the same model can be perceived. Selected results are shown in Figure 5.

While the turbulence model has difficulties adjusting to all of the velocity profiles, the transition model adapts much better to the results, even in the transition region. The part when it distances the most from the experimental results is on the very last profile, where the experimental turbulence profile is steeper than the predicted one.

Regarding the boundary layer displacement thickness and shape factor, the results obtained demonstrate a very similar pattern to the ones obtained in the velocity profiles. The $k - \omega$ SST model has difficulty adjusting to the data, while the $\gamma - \tilde{Re}_{\theta_t}$ model has a considerably better adjustment. The exception to this is the case with $Tu = 1.2\%$, since it presents an underdeveloped turbulent region.

In order to verify these results with other flow quantities, the friction coefficient was plotted. It indicates where the transition in the boundary layer occurs when its value increases significantly, as shown in Figure 4b. The results in the Figure verify the discussions that have been made until now about the results and both models.

As commented previously, the last parameter that was compared to the experimental data were the streamlines on the blade's surface. The analysis

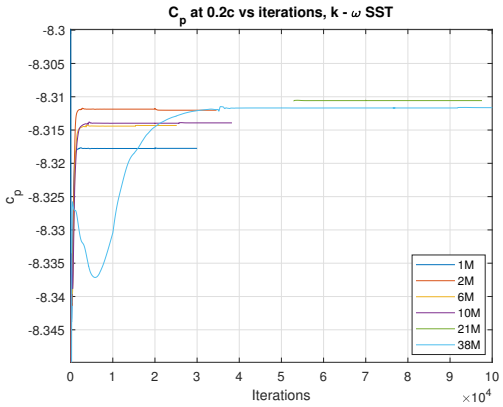

(a) The C_p at $x/c = 0.2$, $k - \omega$ SST model.

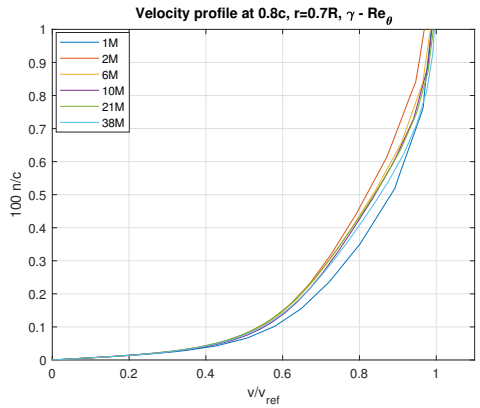

(b) Velocity profile at $x/c = 0.2$, $\gamma - \tilde{Re}_\theta$ model.

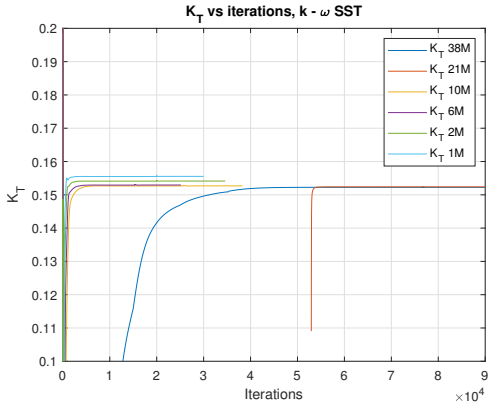

(c) Thrust coefficient vs number of iterations for the $k - \omega$ SST model.

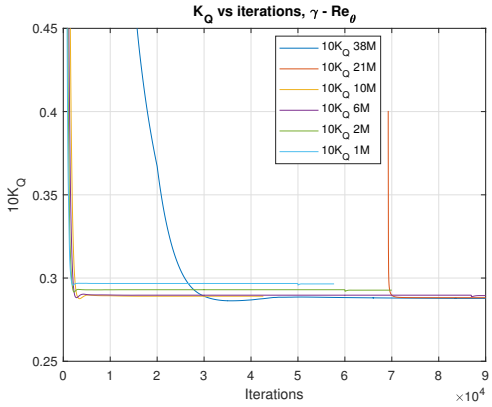

(d) Torque coefficient vs number of iterations for the $\gamma - \tilde{Re}_{\theta t}$ model.

Figure 2: The pressure coefficient, the velocity profiles and the thrust and torque coefficients versus the simulation iterations.

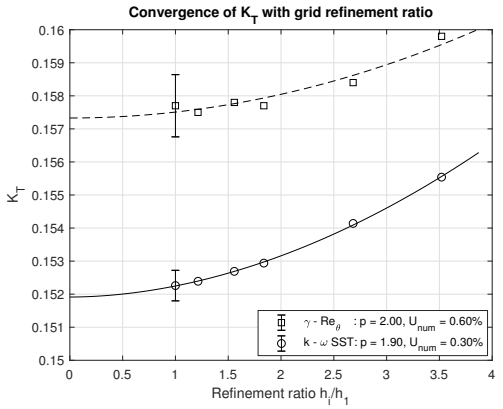

(a) Uncertainty and error estimations for the thrust coefficient K_T.

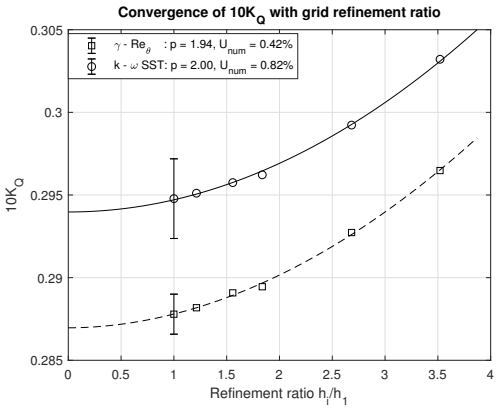

(b) Uncertainty and error estimations for the torque coefficient K_Q.

Figure 3: Results of the Uncertainty and error estimations for the thrust coefficient K_T (left) and the torque coefficient K_Q (right), for both models studied.

of the streamlines suggests the same patterns as the results have shown until now: the transition model is more adjusted to the data compared to the turbulence model. Selected results are shown in Figures 7 and 8.

The red lines in Figure 7a and b indicate the approximate location of the transition region of the boundary layer, which is indicated by a change in the streamlines' direction [21]. As is usual, the $k-\omega$ SST model is not as well-adjusted to the data as is the $\gamma - \tilde{Re}_{\theta_t}$ model, especially the case with $Tu = 1.5\%$ and $Tu = 1.7\%$. For the case with the higher number of Reynolds ($Re = 1.46 \times 10^6$), the

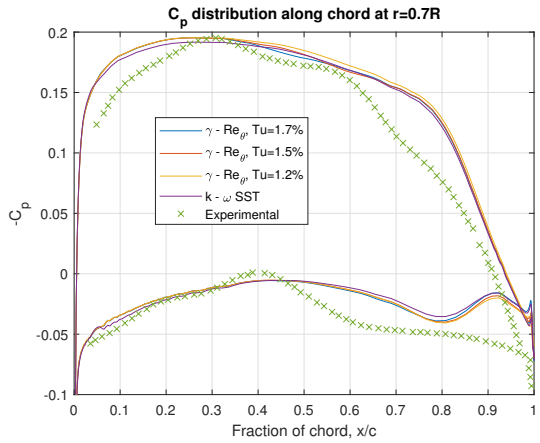

(a) Distribution of the pressure coefficient along the chord at $r = 0.7R$ for the two studied models.

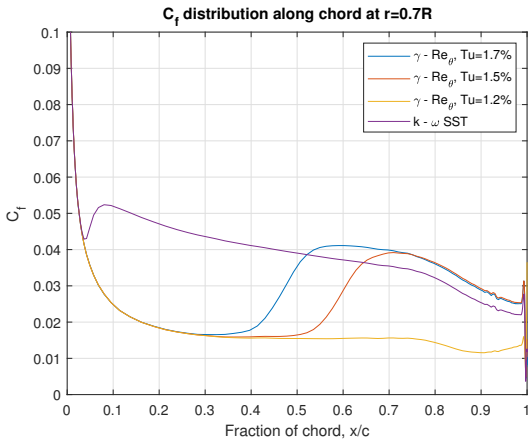

(b) Friction coefficient for both models studied.

Figure 4: The pressure coefficient and the friction coefficient along the chord for all cases studied.

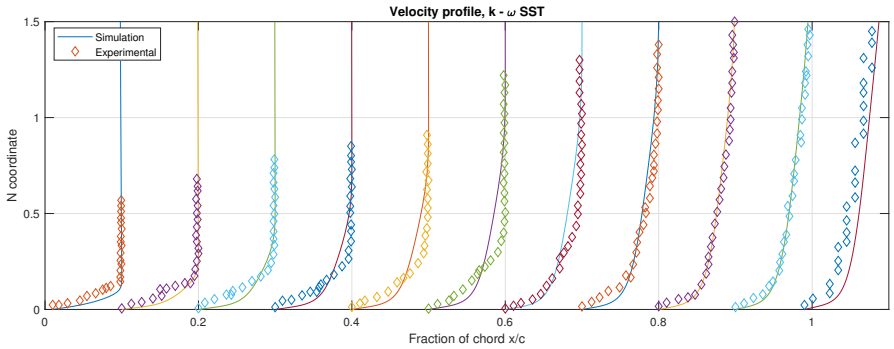

(a) Velocity profiles at $r = 0.7R$ for the $k - \omega$ model.

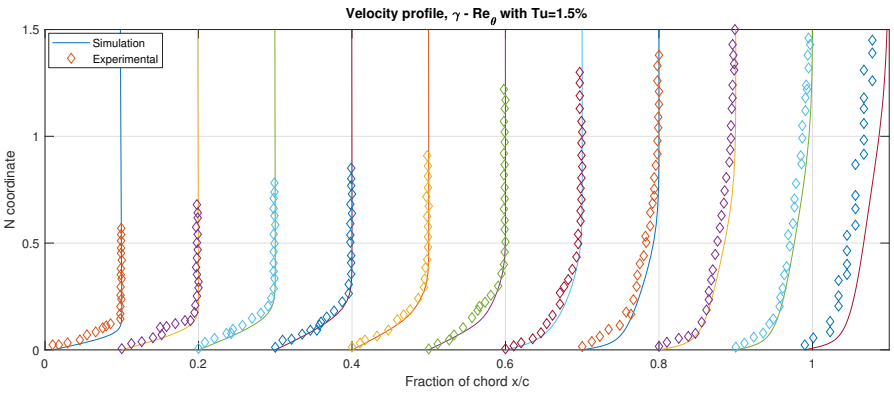

(b) Velocity profiles at $r = 0.7R$ for the $\gamma - \tilde{Re}_{\theta t}$ model and with $Tu = 1.5\%$.

Figure 5: Velocity profiles for the $k - \omega$ SST model and the $\gamma - \tilde{Re}_{\theta t}$ model with $Tu = 1.5\%$.

turbulence model is better adjusted to the streamlines.

5. Conclusions

The results obtained on the numerical analysis have shown that the models used, as well as the solver, give accurate results with very low uncertainty and error, which makes the models very reliable. With that in mind, the parameters considered and analysed in this work presented variations in the results depending on the model used. Most of these variations were not significant (i.e. on the pressure coefficient), and others were clearly more significant (i.e. on the shape factor). Moreover, the $\gamma - \tilde{Re}_{\theta}$ model presented variations with the different turbulence intensities used in the simulations, which makes the results highly dependent on the initial conditions as well as the model employed. That being said, all results obtained are coherent with the experimental data.

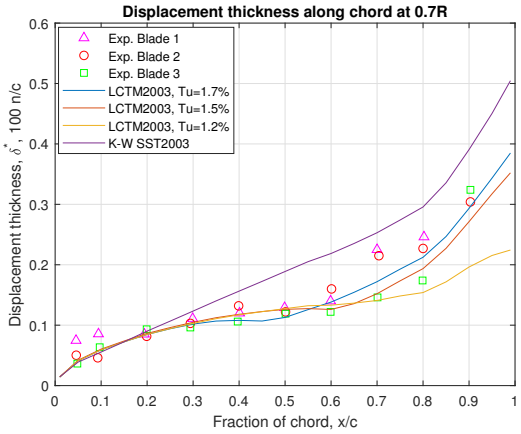

(a) The boundary layer displacement thickness and the experimental data from the literature for both models studied.

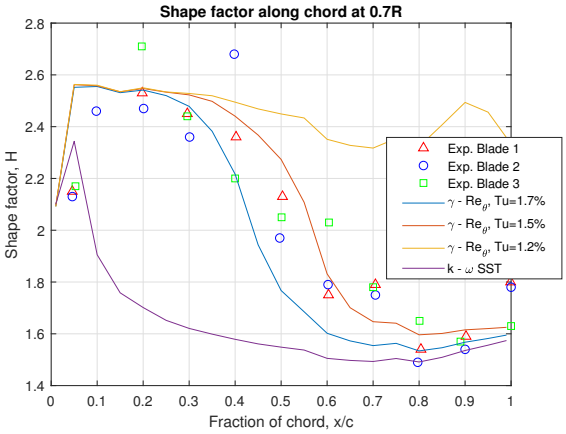

(b) The boundary layer shape factor and the experimental data from the literature for both models studied.

Figure 6: Displacement thickness and shape factor of the boundary layer for the cases studied.

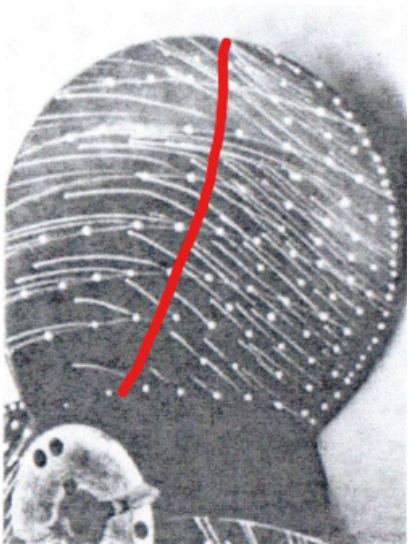

(a) Streamlines from the literature, $Re = 7.3 \times 10^5$, pressure side.

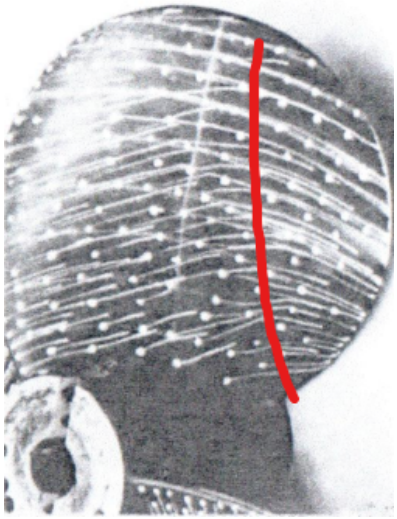

(b) Streamlines from the literature, $Re = 7.3 \times 10^5$, suction side.

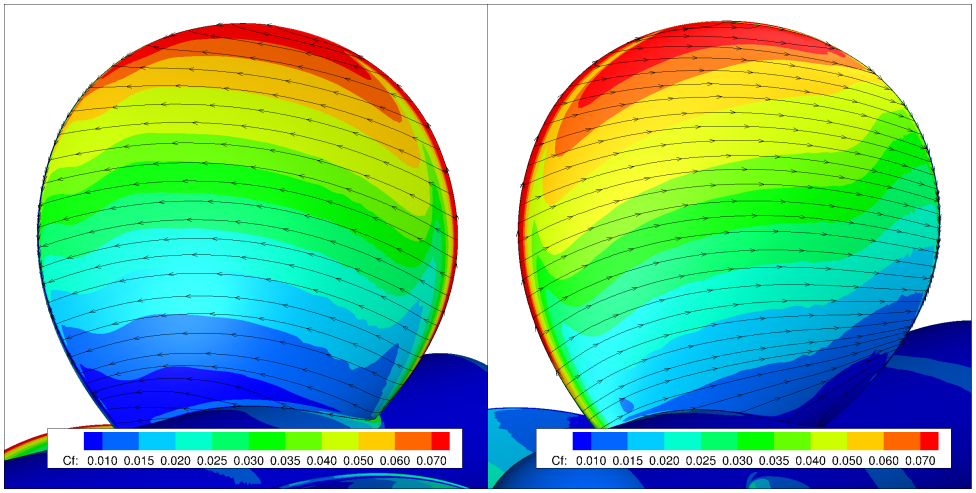

(c) Streamlines obtained from the simulations, $Re = 7.3 \times 10^5$, for the $k - \omega$ model. Left: pressure side. Right: suction side.

Figure 7: Streamlines from both the literature [1] and the simulations for the case $Re = 7.3 \times 10^5$ and the $k - \omega$ model.

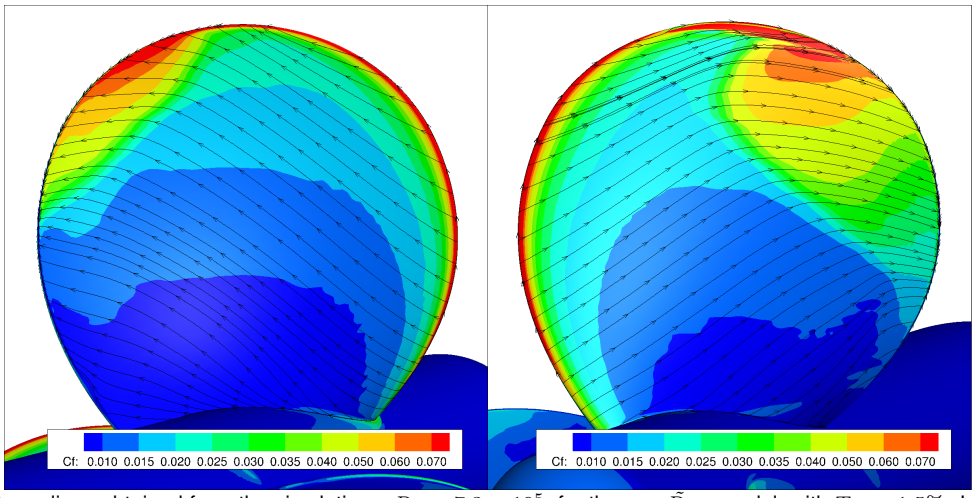

Figure 8: Streamlines obtained from the simulations, $Re = 7.3 \times 10^5$, for the $\gamma - \tilde{Re}_{\theta t}$ model, with $Tu = 1.5\%$. Left: pressure side. Right: suction side.

Regarding the two models used, the $k - \omega$ SST model has proved quite limited in the prediction of the laminar regions of the flow, but excels in the turbulent parts; On the other hand, the $\gamma - \tilde{Re}_{\theta}$ model generally does a better job of this because it accounts for the laminar region and the transition, and is incorporated with the SST model. Overall, the $\gamma - \tilde{Re}_{\theta}$ model is a better choice for this kind of simulations.

Having analysed all of the aforementioned parameters presented in this work, the objectives set in Section 1 are considered to be achieved. Furthermore, all these objectives were achieved with good results.

As a final note, the author would like to propose some future works that can be done in relation to the presented work in this document:

- Perform the same work done in this work with different turbulence model. One model proposed for this use is the modified Spalart-Allmaras one-equation Transition Model [22, 23], since its simplicity would afford quickness in the calculations and the analysis.
- Recreate the experiment of Jessup et al, to confirm the data obtained and also compared to the simulated data obtained in this work.
- Predict the full-scale performance of propeller P4119 studied in this work, with the data obtained by Jessup and the simulated data presented in this work.

Acknowledgements
I would like to thank MARIN for allowing the use of their clusters to perform part of the calculations presented in this work.

References

[1] Stuart D. Jessup, Carl G. Schott, Michael F. Jeffers, and Sukeyuki Kobayashi. Local Propeller Blade Flows in Uniform and Sheared Onset Flows Using LDV Techniques. In *15th Office of Naval Research Symposium*, pages 221–237, 1984.

[2] Amadeo Moran-Guerrero, Juan Gonzalez-Adalid, Mariano Perez-Sobrino, and Leo Gonzalez-Gutierrez. Open Water results comparison for three propellers with transition model, applying crossflow effect, and its comparison with experimental results. In *Fifth International Symposium on Marine Propulsors*, June 2017.

[3] Huilan Yao and Huaixin Zhang. A simple method for estimating transition locations on blade surface of model propellers to be used for calculating viscous force. *International Journal of Naval Architecture and Ocean Engineering*, 10(4):477–490, 2018. `https://doi.org/10.1016/j.ijnaoe.2017.09.002`.

[4] Xiao Wang and Keith Walters. Computational Analysis of Marine-Propeller Performance Using Transition-Sensitive Turbulence Modeling. *Journal of Fluids Engineering*, 134:071107, 07 2012. `https://doi.org/10.1115/1.4005729`.

[5] Mohamed M. Helal, Tamer M. Ahmed, Adel A. Banawan, and Mohamed A. Kotb. Numerical prediction of sheet cavitation on marine propellers using CFD simulation with transition-sensitive turbulence model. *Alexandria Engineering Journal*, 57(4):3805–3815, 2018. `https://doi.org/10.1016/j.aej.2018.03.008`.

[6] Vladimir Krasilnikov, Jiaying Sun, and Karl Henning Halse. Cfd investigation in scale effect on propellers with different magnitude of skew in turbulent flow. In *First International Symposium on Marine Propulsors*, June 2009.

[7] Douwe Rijpkema, João Baltazar, and José Falcão de Campos. Viscous flow simulations of propellers in different reynolds number regimes. In *Fourth International Symposium on Marine Propulsors*, June 2015.

[8] P. A. Costa Rocha, H. H. Barbosa Rocha, F. O. Moura Carneiro, M. E. Vieira da Silva, and C. Freitas de Andrade. A case study on the calibration of the $k-\omega$ SST (shear stress transport) turbulence model for small scale wind turbines designed with cambered and symmetrical airfoils. *Energy Journal*, 97:144–150, December 2019. https://doi.org/10.1016/j.energy.2015.12.081.

[9] Ioannis Bouras, Lin Ma, Derek Ingham, and Mohamed Pourkashanian. An improved k–ω turbulence model for the simulations of the wind turbine wakes in a neutral atmospheric boundary layer flow. *Journal of Wind Eningeering and Industrial Aerodynamics*, 179:358–368, June 2018. https://doi.org/10.1016/j.jweia.2018.06.013.

[10] Aldo Rona, M.F.F. El-Dosoky, and D.S. Adebayo. A hybrid rans model of wing-body junction flow. *European Journal of Mechanics - B/Fluids*, 79:283 – 296, 2020.

[11] F. Rizzo, V. D'Alessandro, S. Montelpare, and L. Giammichele. Computational study of a bluff body aerodynamics: Impact of the laminar-to-turbulent transition modelling. *International Journal of Mechanical Sciences*, 178:105620, March 2020. https://doi.org/10.1016/j.ijmecsci.2020.105620.

[12] F.R. Menter, M. Kuntz, and R. Langtry. Ten Years of Industrial Experience with the SST Turbulence Model. In Begell House Inc, editor, *4th International Symposium on Turbulence, Heat and Mass Transfer*, volume 4, pages 625–632, 2003.

[13] Robin Blair Langtry. *A Correlation-Based Transition Model using Local Variables for Unstructured Parallelized CFD codes*. PhD thesis, Institut für Thermische Strömungsmaschinen und Maschinenlaboratorium - Universität Stuttgart, May 2006.

[14] Robin B. Langtry and Florian R. Menter. Correlation-based transition modeling for unstructured parallelized computational fluid dynamics codes. *American Institute of Aeronautics and Astronautics Journal*, 47:2894–2906, 2009. https://doi.org/10.2514/1.42362.

[15] Stephen B. Denny. *Cavitation and Open-Water performance tests of a series of propellers designed by lifting-surface methods*. Department of the Navy– Naval Ship Research and Development Center, Washington D.C. 20007, September 1968.

[16] João Baltazar, Douwe Rijpkema, and José Falcão de Campos. On the use of the gamma - re theta transition model for the prediction of the propeller performance at model-scale. *Ocean Engineering*, 170:6–19, 2018. https://doi.org/10.1016/j.oceaneng.2018.10.005.

[17] Maritime Research Institute Netherlands, 6700 AA Wagenringen, The Netherlands. *ReFRESCO Theory Manual*, 2.4.0 edition, October 2017.

[18] F. R. Menter. Two-equation eddy-viscosity turbulence models for engineering applications. *American Institute of Aeronautics and Astronautics Journal*, 32:1598–1605, 1994. https://doi.org/10.2514/3.12149".

[19] L. Eça and M. Hoekstra. Verification and Validation for Marine Applications of CFD. In *20th Symposium on Naval Hydrodynamics*, August 2012.

[20] L. Eça and M. Hoekstra. A procedure for the estimation of the numerical uncertainty of CFD calculations based on grid refinement studies. *Journal of Computational Physics*, 262:104–130, 2014. https://dx.doi.org/10.1016/j.jcp.2014.01.006.

[21] Gerrit Kuiper. *Cavitation inception on ship propeller models*. PhD thesis, Technische Hogeschool Delft, 1981.

[22] Samet C. Cakmakcioglu, Onur Bas, Riccardo Mura, and Unver Kaynak. Ta revised one-equation transitional model for external aerodynamics. In *AIAA Aviation Forum*, 2020.

[23] Aldo Rona, M.F.F. El-Dosoky, and D.S. Adebayo. A revised one-equation transitional model for external aerodynamics. *AIAA Paper*, 79:2020–2076, 2020.